



UvA-DARE (Digital Academic Repository)

Multi-modal ultra-high resolution structural 7-Tesla MRI data repository

Forstmann, B.U.; Keuken, M.C.; Schafer, A.; Bazin, P.-L.; Alkemade, A.; Turner, R.

DOI

[10.1038/sdata.2014.50](https://doi.org/10.1038/sdata.2014.50)

Publication date

2014

Document Version

Final published version

Published in

Scientific Data

License

CC BY

[Link to publication](#)

Citation for published version (APA):

Forstmann, B. U., Keuken, M. C., Schafer, A., Bazin, P.-L., Alkemade, A., & Turner, R. (2014). Multi-modal ultra-high resolution structural 7-Tesla MRI data repository. *Scientific Data*, 1, Article 140050. <https://doi.org/10.1038/sdata.2014.50>

General rights

It is not permitted to download or to forward/distribute the text or part of it without the consent of the author(s) and/or copyright holder(s), other than for strictly personal, individual use, unless the work is under an open content license (like Creative Commons).

Disclaimer/Complaints regulations

If you believe that digital publication of certain material infringes any of your rights or (privacy) interests, please let the Library know, stating your reasons. In case of a legitimate complaint, the Library will make the material inaccessible and/or remove it from the website. Please Ask the Library: <https://uba.uva.nl/en/contact>, or a letter to: Library of the University of Amsterdam, Secretariat, P.O. Box 19185, 1000 GD Amsterdam, The Netherlands. You will be contacted as soon as possible.

SCIENTIFIC DATA

OPEN

SUBJECT CATEGORIES

» Neuroscience

» Cognitive Neuroscience

Multi-modal ultra-high resolution structural 7-Tesla MRI data repository

Birte U. Forstmann^{1,2}, Max C. Keuken^{1,2}, Andreas Schafer², Pierre-Louis Bazin², Anneke Alkemade¹ & Robert Turner²

Received: 11 July 2014

Accepted: 05 November 2014

Published: 9 December 2014

Structural brain data is key for the understanding of brain function and networks, i.e., connectomics. Here we present data sets available from the 'atlasing of the basal ganglia (ATAG)' project, which provides ultra-high resolution 7 Tesla (T) magnetic resonance imaging (MRI) scans from young, middle-aged, and elderly participants. The ATAG data set includes whole-brain and reduced field-of-view MP2RAGE and T2*-weighted scans of the subcortex and brainstem with ultra-high resolution at a sub-millimeter scale. The data can be used to develop new algorithms that help building high-resolution atlases both relevant for the basic and clinical neurosciences. Importantly, the present data repository may also be used to inform the exact positioning of electrodes used for deep-brain-stimulation in patients with Parkinson's disease and neuropsychiatric diseases.

Design Type(s)	parallel group design • observation design
Measurement Type(s)	nuclear magnetic resonance assay
Technology Type(s)	MRI Scanner
Factor Type(s)	age
Sample Characteristic(s)	Homo sapiens • brain

¹Amsterdam Center for Brain & Cognition, University of Amsterdam, 1018 WS Amsterdam, Netherlands. ²Max Planck Institute for Human Cognitive and Brain Sciences, 04103 Leipzig, Germany.

Correspondence and requests for materials should be addressed to B.U.F. (email: buforstmann@gmail.com)

Background & Summary

Large collaborative projects between scientific groups spread around the world are aimed to increase our understanding of the human brain. Large human connectome studies^{1–3} are in place working to clarify the connectivity within the human brain using a multi-modal approach ranging from structural brain imaging to genetics (<http://www.humanconnectomeproject.org>). However, to fully understand the connectivity of the brain, we need a higher level of anatomical detail than currently available. The lack of knowledge about small brain structures, especially subcortical structures, is reflected by their absence from brain atlases currently available for MRI research^{4,5}. A comparison of subcortical grey matter structures depicted in standard MRI-atlases with the structures defined in the Federative Community on Anatomical Terminology⁶ yielded an overlap of only seven percent. One important explanation for this discrepancy is the absence of ultra-high resolution MRI data allowing the direct visualization of small nuclei in the subcortex. A second important reason is the lack of automated analytical protocols available for MRI-data segmentation, with the resulting necessity of laborious studies performed by trained anatomists for the identification of subcortical brain areas. Thirdly, besides the lack of anatomical knowledge, there is no information about age-related changes in, e.g., volume or location of subcortical structures.

Recent exciting advancements in the field of ultra-high resolution magnetic resonance imaging at 7 Tesla (or higher) allow *in vivo* neuroimaging of the human brain with unprecedented anatomical detail^{7–11}. Here we share information of a multi-modal data set of three different groups of young, middle-aged, and elderly participants who were scanned with a 7 T MRI scanner. The data sets contain three different age groups and can be used to investigate anatomical changes due to healthy aging. The data sets have already been used to create probabilistic atlas maps including the striatum, globus pallidus interna and externa, the substantia nigra, the subthalamic, and the red nucleus. All probabilistic atlas maps are available online (<https://www.nitrc.org/projects/atag/> and <http://fsl.fmrib.ox.ac.uk/fsl/fslwiki/Atlases>). In addition to the manual segmentations, the data can be used to develop new algorithms that help building high-resolution subcortical brain atlases that can be directly applied in both the basic and clinical neurosciences. Finally, the data can be used to guide the exact positioning of electrodes relevant for deep-brain-stimulation often used in patients with Parkinson's disease and neuropsychiatric diseases^{12–14}.

Methods

Participants

For the acquisition of the structural brain scans, 30 young participants (14 females) with mean age 23.8 (s.d. 2.3), 14 middle-aged (7 females) with mean age 52.5 (s.d. 6.6), and 10 elderly (3 females) with mean age 69.6 (s.d. 4.6) were included (Table 1). All participants had normal or corrected-to-normal vision, and none of them suffered from neurological, psychiatric, or somatic diseases. All subjects were right-handed, as confirmed by the Edinburgh Inventory¹⁵. The study was approved by the local ethics committee at the University of Leipzig, Germany. All participants gave their written informed consent prior to scanning and received a monetary compensation.

Scan parameters

The structural data were acquired using a 7 T Siemens Magnetom MRI scanner using a 24-channel head array Nova coil (NOVA Medical Inc., Wilmington MA) and consisted of three sequences: a whole-brain MP2RAGE, a MP2RAGE covering a smaller slab^{16,17}, and a multi-echo 3D FLASH¹⁸. The whole-brain MP2RAGE had 240 sagittal slices with an acquisition time of 10:57 min (repetition time (TR) = 5,000 ms; echo time (TE) = 2.45 ms; inversion times T11/T12 = 900/2,750 ms; flip angle = 5°/3°; bandwidth = 250 Hz/Px; voxel size = (0.7 mm)³; Table 2 (available online only)). The MP2RAGE slab consisted of 128 slices with an acquisition time of 9:07 min (TR = 5,000 ms; TE = 3.71 ms; T11/T12 = 900/2,750 ms; flip angle = 5°/3°; bandwidth = 240 Hz/Px; voxel size = (0.6 mm)³; Table 3 (available online only)). The FLASH slab consisted of 128 slices with an acquisition time of 17:18 min (TR = 41 ms and three different echo times (TE): 11.22/20.39/29.57 ms; flip angle = 14°; bandwidth = 160 Hz/Px; voxel size = (0.5 mm)³; Table 4 (available online only)). Both slab sequences consisted of axial slices tilted –23 degrees to the true axial plane in scanner coordinates. This angle in combination with the used field of view ensured that the entire Basal Ganglia were scanned. To get a better inversion of the magnetization in the lower parts of the brain (e.g., the Cerebellum), a TR-FOCI inversion pulse was implemented in the MP2RAGE sequence¹⁶.

Unless indicated otherwise, all MRI data files were converted from DICOM to NIfTI format using an in-house dicom-to-nifti converter. This linux compatible converter is available via <https://github.com/isis-group/isis>.

Scan volumes

The MP2RAGE sequence results in four different volumes for each subject: INV1, INV2, UNI and T1. The INV1 volume reflects the gradient echo sequence with an inversion time of 900 ms. The INV2 volume reflects the gradient echo sequence with an inversion time of 2,750 ms. The UNI volume is the combined volume of the two inversion times. Finally, the T1 volume is a T1 estimation map derived from the two inversion times (Marques *et al.*¹⁷). The FLASH sequence results in two different volumes per echo time per subject resulting in nine different volumes in total. Besides the standard T2* weighted

Age Group	Participant	Gender	Age
1	pp01	Female	23
	pp02	Female	23
	pp03	Female	25
	pp04	Female	23
	pp05	Male	27
	pp06	Female	23
	pp07	Male	27
	pp08	Female	24
	pp09	Male	24
	pp10	Male	22
	pp11	Female	25
	pp12	Female	24
	pp13	Male	24
	pp14	Male	26
	pp15	Male	23
	pp16	Female	25
	pp17	Female	19
	pp18	Male	23
	pp19	Male	21
	pp20	Male	25
	pp21	Male	24
	pp22	Male	28
	pp23	Male	28
	pp24	Female	22
	pp25	Female	19
	pp26	Female	21
	pp27	Male	25
	pp28	Female	21
	pp29	Male	26
	pp30	Male	23
2	pp31	Female	56
	pp32	Female	60
	pp33	Female	58
	pp34	Male	40
	pp35	Male	42
	pp36	Male	60
	pp37	Female	59
	pp38	Female	49
	pp39	Female	45
	pp40	Female	55
	pp41	Male	55
	pp42	Male	49
	pp43	Male	54
	pp44	Male	53
3	pp45	Female	74
	pp46	Male	63
	pp47	Female	62
	pp48	Male	72
	pp49	Male	67
	pp50	Male	75
	pp51	Male	69
	pp52	Male	68
	pp53	Female	73

Table 1. Demographic information of participants.

magnitude image, the phase images are also provided and can be used to calculate susceptibility weighted images as well as quantitative susceptibility maps (e.g., Deistung *et al.*¹⁹).

Data processing

All structural scans were anonymized by zeroing out the voxels in the vicinity of the facial surface, teeth, and auricles following a similar procedure as described by Hanke *et al.*²⁰ All data were reoriented to the standard MNI space using the `fslreorient2std` tool as implemented in `fslutils` 5.0.2 (Figure 1).

Data Records

All data records listed in this section are available from NITRIC (Data Citation 1) or Dryad (Data Citation 2). A README file with a detailed description of the content of all downloads is available in Dryad. Additional material and information are also provided in Data Citation 1 and Data Citation 2.

Unless noted otherwise, all MRI data files were converted from DICOM to NIfTI format using an in-house `dicom-to-nifti` converter. In order to de-identify data, information on centre-specific study and participant codes have been removed using an automated procedure. All human participants were given sequential integer IDs.

Technical Validation

Motion artifacts

In line with Gedamu *et al.*²¹, motion artifacts in the structural volumes were estimated by calculating the noise ratio between the phase encoding direction and read direction outside of the brain. Two ROIs of $\pm 1,225 \text{ mm}^2$ was drawn in the sagittal plane; 5 mm lateral of the skull, and in the coronal plane; 5 mm anterior of the skull, in the magnitude image of the second inversion time of the MP2RAGE sequence and FLASH sequences. The sagittal ROI corresponds to the read direction for the MP2RAGE whole brain and phase encoding direction for the MP2RAGE and FLASH slab, whereas the coronal ROI corresponds to the phase encoding direction for the MP2RAGE whole brain and read direction for the MP2RAGE and FLASH slab. The mean signal was extracted from both ROI's and the mean phase encoding direction signal was divided by the mean read direction signal. The closer this ratio is to 1, the less motion artifacts are present. Following Gedamu *et al.*²¹, we estimated that any ratio below 2 reflects little to no motion artifacts (see Figure 2 for an example of the data quality).

One sided *t*-tests were conducted to test whether any of the groups showed significant motion artifacts in any of the sequences. All ratios per sequence and age group were significantly lower than 2 (MP2RAGE whole-brain: young ($t(29) = -17.93$, $P < 0.001$); middle-aged ($t(13) = -5.44$, $P < 0.001$); elderly ($t(8) = -7.19$, $P < 0.001$), MP2RAGE slab: young ($t(29) = -35.06$, $P < 0.001$); middle-aged ($t(13) = -23.43$, $P < 0.001$); elderly ($t(8) = -13.33$, $P < 0.001$), FLASH echo 1: young ($t(29) = -3.74$, $P < 0.001$); middle-aged ($t(13) = -17.68$, $P < 0.001$); elderly ($t(8) = -16.97$, $P < 0.001$), FLASH echo 2: young ($t(29) = -6.88$, $P < 0.001$); middle-aged ($t(13) = -14.88$, $P < 0.001$); elderly ($t(8) = -6.31$, $P < 0.001$), FLASH echo 3: young ($t(29) = -10.36$, $P < 0.001$); middle-aged ($t(13) = -6.23$, $P < 0.001$); elderly ($t(8) = -19.53$, $P < 0.001$); Table 5 (available online only)).

There was no main effect of age on motion for the MP2RAGE whole brain ($F(2,50) = 1.29$, $P = 0.29$) or MP2RAGE slab ($F(2,50) = 0.8$, $P = 0.44$). There was a main effect of age and echo time on motion for the FLASH sequence (age: $F(2,147) = 4.97$, $P = 0.008$, echo time: $F(2,147) = 10.45$, $P < 0.001$). *Post-hoc* testing showed that the young had significantly more motion artifacts than both the middle-aged and elderly (young versus middle-aged: $t(103.18) = 5.61$, $P < 0.001$, young versus elderly: $t(79.03) = 5.25$, $P < 0.001$) whereas the middle-aged and elderly did not differ significantly ($t(65.73) = -0.59$, $P = 1.0$). *Post-hoc* testing showed that the first echo time had significantly less motion artifacts than both the second and third echo time (first echo versus second echo: $t(90) = -3.29$, $P = 0.003$, first echo versus third echo: $t(82.17) = -3.77$, $P = 0.001$) whereas the second and third echo time did not differ significantly ($t(101.66) = -0.72$, $P = 0.92$). All *post-hoc* testing was Bonferroni corrected at an alpha of 0.05.

Signal to noise ratio

To estimate the Signal to Noise Ratio (SNR), the mean signal from an axial slice just above the corpus callosum was divided by the standard deviation of the signal in the read direction ROI both in the magnitude image of the second inversion time of the MP2RAGE sequence and FLASH sequences. To improve the estimation of noise a Rician correction was applied²². As this is still an approximation of the true SNR, the term $\text{SNR}_{\text{approx}}$ is used. For the three different sequences there was a main effect of age on $\text{SNR}_{\text{approx}}$ (MP2RAGE whole brain: $F(2,50) = 48.3$, $P < 0.001$; MP2RAGE slab: $F(2,50) = 5.94$, $P = 0.005$; FLASH: $F(2,147) = 6.90$, $P = 0.001$). Additionally there was a main effect of echo time on $\text{SNR}_{\text{approx}}$ ($F(2,147) = 11.75$, $P < 0.001$).

Post-hoc testing showed that for the MP2RAGE whole brain, the young had a significantly higher $\text{SNR}_{\text{approx}}$ than both the middle-aged and elderly (young versus middle-aged: $t(33.72) = 8.87$, $P < 0.001$; young versus elderly: $t(18.37) = 8.41$, $P < 0.001$) whereas the middle-aged and elderly did not differ significantly ($t(17.61) = 0.46$, $P = 1.0$). A similar pattern was found for the MP2RAGE slab. The young had a significantly higher $\text{SNR}_{\text{approx}}$ than both the middle-aged and elderly (young versus middle-aged: $t(24.8) = 2.86$, $P = 0.017$; young versus elderly: $t(17.46) = 2.92$, $P = 0.019$) whereas the middle-aged and elderly did not differ significantly ($t(20.56) = -0.10$, $P = 1.0$). The young had a significantly higher

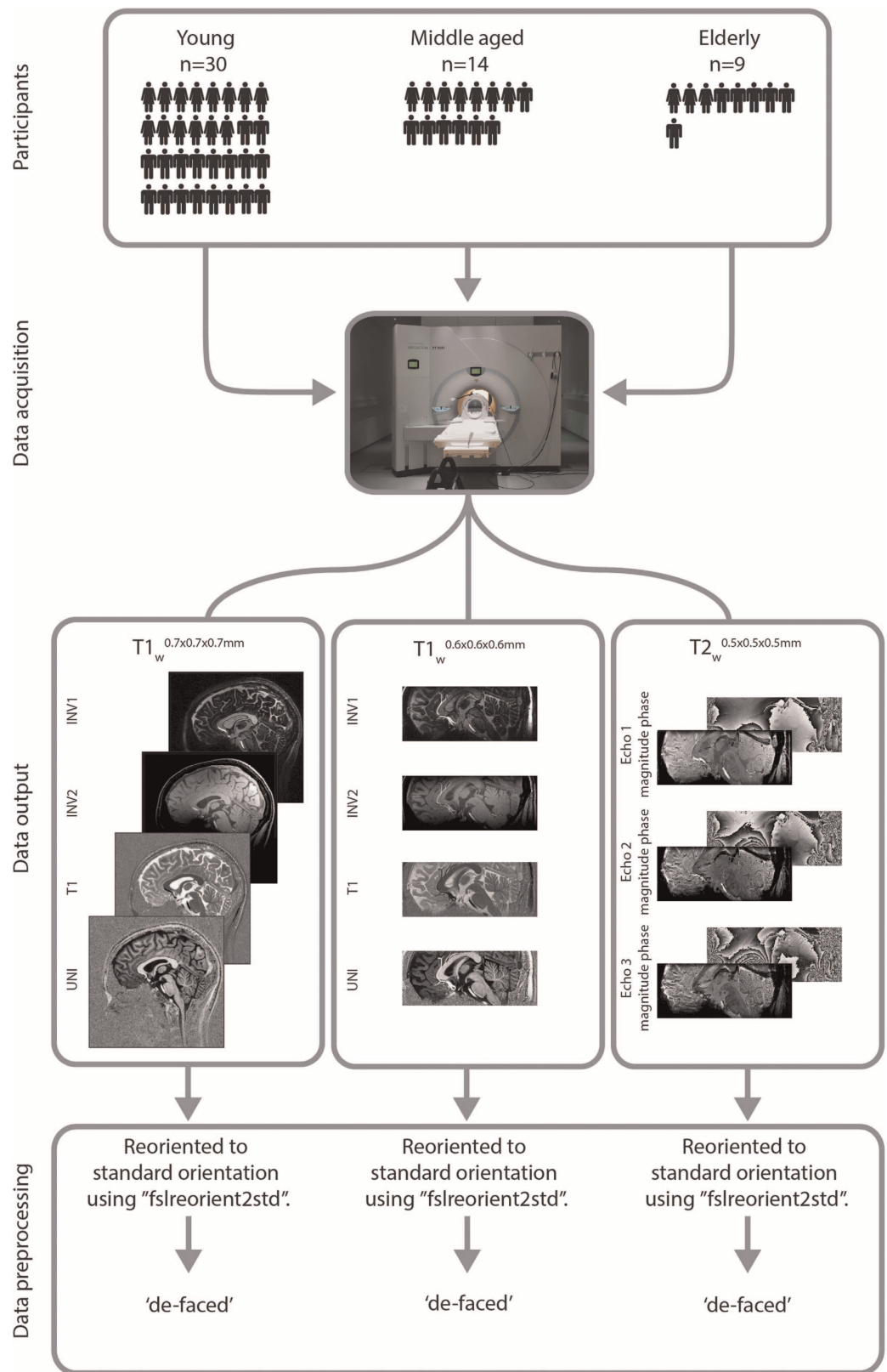


Figure 1. Data acquisition workflow. Three different age groups were structurally scanned using a 7 T MRI scanner. Data acquisition was done in a single imaging session that lasted for approximately 37 min. This resulted in three different datasets: a whole brain T1-weighted MP2RAGE volume; a slab T1-weighted MP2RAGE volume, and a T2*-weighted flash volume. All structural data was anonymized and reoriented to standard MNI orientation (7 T MRI photo courtesy of Andreas Döring).

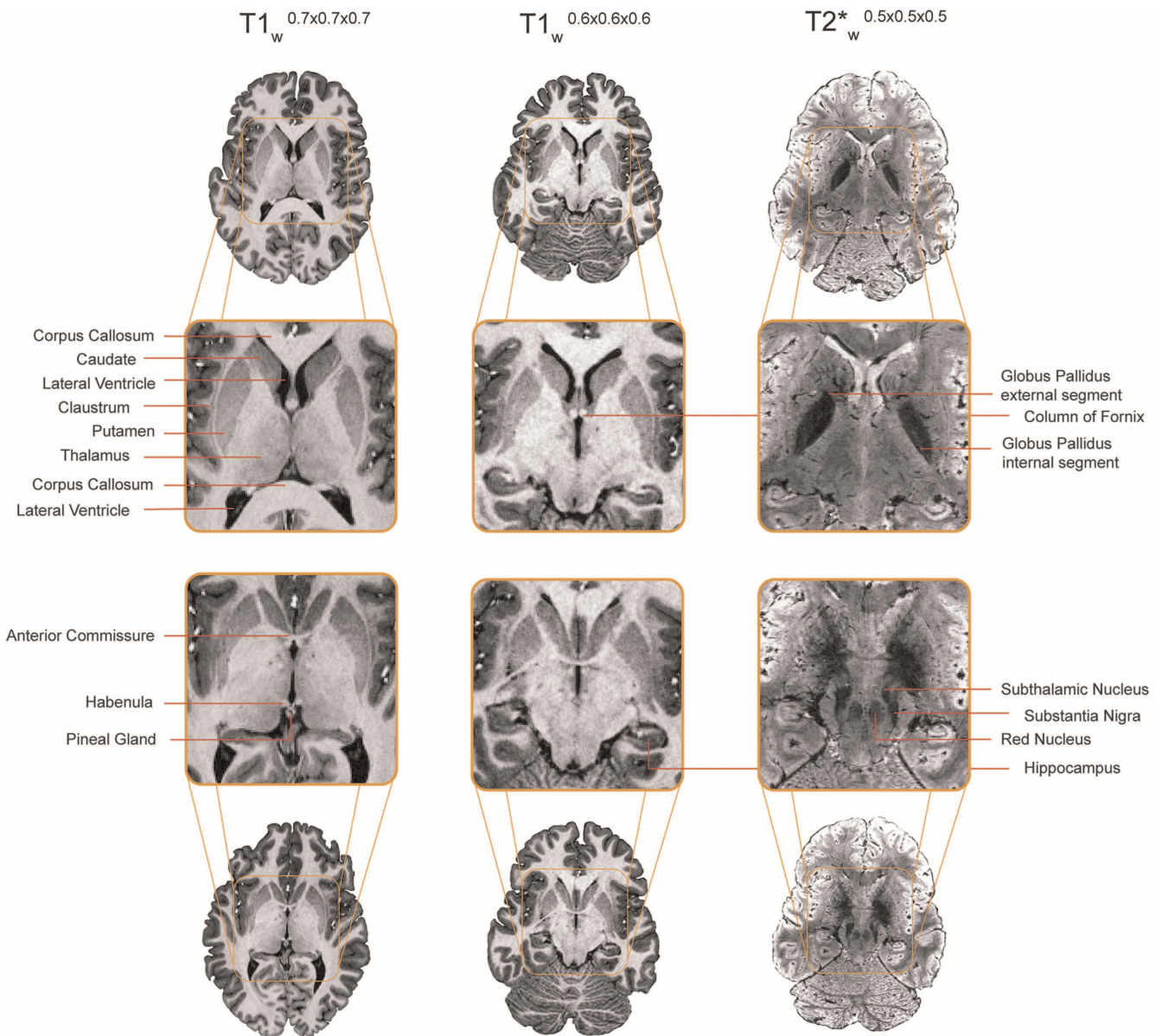


Figure 2. An example of the data quality. Two axial images of the three acquired datasets are displayed for a representative young subject. Only a few of the easily identifiable structures have been labeled. Note that not all structures are equally well visible in the T1-weighted volumes compared to the T2*-weighted volume and argue for the need of multi sequence acquisition when interested in subcortical structures.

SNR_{approx} in the FLASH sequence than the middle-aged ($t(70.80) = 3.35$, $P = 0.003$) but did not differ from the elderly ($t(36.31) = 0.16$, $P = 1.0$). The middle-aged and elderly did not differ in SNR_{approx} for the FLASH sequence ($t(51.87) = -2.16$, $P = 0.071$). *Post-hoc* testing showed that the first echo time had significantly more SNR_{approx} than both the second and third echo time (first echo versus second echo: $t(97.2) = 4.89$, $P < 0.001$, first echo versus third echo: $t(88.4) = 8.05$, $P < 0.001$). The second echo time had significantly higher SNR_{approx} than the third echo time ($t(100.91) = 3.42$, $P = 0.002$). All *post-hoc* testing was Bonferroni corrected at an alpha of 0.05 (Table 6 (available online only)).

In addition to the SNR_{approx} calculation and the noise ratio between the phase encoding direction and read direction, the scans were visually inspected by two independent researchers. The FLASH magnitude scans were checked for ghosting, wrapping, or shading artifacts. The MP2RAGE UNI scans were checked for ghosting, wrapping, shading, and the presence of 'zebra stripe' artifacts. Finally the MP2RAGE T1 scans were checked for ghosting, wrapping, shading, the presence of 'zebra stripes', and CSF clipping artifacts where '1' corresponds to not present at all and '5' corresponds to severely present.

Ghosting artifacts are generally caused by motion and appear as a 'ghost' image of the brain in phase encoding direction. Wrapping artifacts are usually caused by anatomical features protruding outside of

the imaged field of view but still within the sensitive volume of the RF coil. Shading artifacts were defined as a non-homogenous intensity throughout the entire brain. Zebra stripes were defined as well defined alternating black and white stripes present in the brain. Finally, CSF clipping artifacts were defined as the voxels in the CSF that have a signal dropout and appear black (McRobbie *et al.*, 2006).

The mean rating for each scale for each checked volume is given in Table 7 (available online only). Volumes that had a higher rating on that quality check than the rest of the age group based on the $\pm 1.5^*$ interquartile range are highlighted with an asterisk.

As a result of the scan parameters of the MP2RAGE sequence, a number of participants show T1 clipping artifacts in the T1 map located in the CSF. This is indicated in Table 7 (available online only). Note that these clipping artifacts do not affect the T1 values reported in the grey and white matter tissue.

Usage Notes

The procedures we employed in this study resulted in a dataset that is highly suitable for automated processing. Data are shared in documented standard formats, such as NIfTI or plain text files, to enable further processing in arbitrary analysis environments with no imposed dependencies on proprietary tools. All processing performed on the released data article were produced by open-source software on standard computer workstations.

References

1. Biswal, B. B. *et al.* Toward discovery science of human brain function. *Proc. Natl Acad. Sci.* **107**, 4734–4739 (2010).
2. Sporns, O., Tononi, G. & Kötter, R. The Human Connectome: A structural description of the human brain. *PLoS Comp. Biol.* **1**, e42 (2005).
3. Van Essen, D. C. *et al.* The Human Connectome Project: A data acquisition perspective. *NeuroImage* **62**, 2222–2231 (2012).
4. Evans, A. C., Janke, A. L., Collins, D. L. & Baillet, S. Brain templates and atlases. *NeuroImage* **62**, 911–922 (2012).
5. Alkemade, A., Keuken, M. C. & Forstmann, B. U. A perspective on terra incognita: uncovering the neuroanatomy of the human subcortex. *Frontiers in Neuroanatomy* **7**, 40 (2013).
6. Federative Committee on Anatomical Terminology. *Terminologia Anatomica* 1–292 (Thieme Stuttgart, 1998).
7. Lenglet, C. *et al.* Comprehensive in vivo mapping of the human basal ganglia and thalamic connectome in individuals using 7T MRI. *PLoS one* **7**, e29153 (2012).
8. Keuken, M. C. *et al.* Quantifying inter-individual anatomical variability in the subcortex using 7T structural MRI. *NeuroImage* **94**, 1–7 (2014).
9. Cho, Z. H. *et al.* New brain atlas—Mapping the human brain in vivo with 7.0 T MRI and comparison with postmortem histology: Will these images change modern medicine? *Int. J. Imag. Syst. Tech.* **18**, 2–8 (2008).
10. Turner, R. in *High-Field MR Imaging* (Springer, 2011).
11. Bazin, P.-L. *et al.* A computational framework for ultra-high resolution cortical segmentation at 7Tesla. *NeuroImage* 1–9 (2013).
12. Beisteiner, R. *et al.* Clinical fMRI: Evidence for a 7T benefit over 3T. *NeuroImage* **57**, 1015–1021 (2011).
13. Cho, Z. H. *et al.* Direct visualization of deep brain stimulation targets in Parkinson disease with the use of 7-tesla magnetic resonance imaging. *J. Neurosurg.* **113**, 1–9 (2010).
14. Abosch, A., Yacoub, E., Ugurbil, K. & Harel, N. An assessment of current brain targets for deep brain stimulation surgery with susceptibility-weighted imaging at 7-tesla. *Neurosurgery* **67**, 1745–1756 (2010).
15. Oldfield, R. C. The assessment and analysis of handedness: the Edinburgh inventory. *Neuropsychologia* **9**, 97–113 (1971).
16. Hurley, A. C. *et al.* Tailored RF pulse for magnetization inversion at ultrahigh field. *Magn. Reson. Med.* **63**, 51–58 (2009).
17. Marques, J. P. *et al.* MP2RAGE, a self bias-field corrected sequence for improved segmentation and T1-mapping at high field. *NeuroImage* **49**, 1271–1281 (2010).
18. Haase, A., Frahm, J., Matthaei, D., Hancic, W. & Merboldt, K. D. FLASH imaging. Rapid NMR imaging using low flip-angle pulses. *J. Magn. Reson.* **67**, 258–266 (1986).
19. Deistung, A. *et al.* Toward in vivo histology: A comparison of quantitative susceptibility mapping (QSM) with magnitude-, phase-, and R2*-imaging at ultra-high magnetic field strength. *NeuroImage* **65**, 299–314 (2013).
20. Hanke, M. *et al.* A high-resolution 7-Tesla fMRI dataset from complex natural stimulation with an audio movie. *Sci. Data* **1**, 140003 (2014).
21. Gedamu, E. L., Collins, D. L. & Arnold, D. L. Automated quality control of brain MR images. *J. Magn. Reson. Imaging* **28**, 308–319 (2008).
22. Gudbjartsson, H. & Patz, S. The Rician distribution of noisy MRI data. *Magn. Reson. Med.* **34**, 910–914 (1995).

Data Citations

1. Forstmann, B. U. *et al.* NITRC www.nitrc.org/projects/atag_mri_scans/ (2014).
2. Forstmann, B. U. *et al.* Dryad <http://doi.org/10.5061/dryad.fb41s> (2014).

Acknowledgements

We thank Domenica Wilfling and Elisabeth Wladimirov for taking such good care of all our participants. This research line is financially supported by the European Research Council (BUF).

Author Contributions

B.U.F. conceived the study and wrote the manuscript. M.C.K. contributed to the manuscript, performed the technical validation, and visually checked the data. A.S. contributed to the manuscript and performed the technical validation. P.-L.B. contributed to the manuscript and provided conceptual discussion. A.A. contributed to the manuscript and visually checked the data. R.T. provided conceptual discussion and contributed to the manuscript.

Additional information

Tables 2–7 are only available in the online version of this paper.

Competing financial interests: The authors declare no competing financial interest.

How to cite this article: Forstmann, B. U. *et al.* Multi-modal ultra-high resolution structural 7-Tesla MRI data repository. *Sci. Data* 1:140050 doi: 10.1038/sdata.2014.50 (2014).



This work is licensed under a Creative Commons Attribution 4.0 International License. The images or other third party material in this article are included in the article's Creative Commons license, unless indicated otherwise in the credit line; if the material is not included under the Creative Commons license, users will need to obtain permission from the license holder to reproduce the material. To view a copy of this license, visit <http://creativecommons.org/licenses/by/4.0>

Metadata associated with this Data Descriptor is available at <http://www.nature.com/sdata/> and is released under the CC0 waiver to maximize reuse.